Image blurring due to turbulent wakes for airborne systems: simulation and modeling

Diskin, Yakov, Goorskey, David, Whiteley, Matthew, Drye, Richard, De Lucca, Nicholas, et al.

Yakov Diskin, David Goorskey, Matthew Whiteley, Richard Drye, Nicholas De Lucca, Stanislav Gordeyev, Eric Jumper, "Image blurring due to turbulent wakes for airborne systems: simulation and modeling," Proc. SPIE 10408, Laser Communication and Propagation through the Atmosphere and Oceans VI, 104080N (30 August 2017); doi: 10.1117/12.2275648

SPIE.

Event: SPIE Optical Engineering + Applications, 2017, San Diego, California, United States

IMAGE BLURRING DUE TO TURBULENT WAKES FOR AIRBORNE SYSTEMS: SIMULATION AND MODELING

Yakov Diskin[a], David Goorskey[a], Matthew Whiteley[a], Richard Drye[a], Nicholas DeLucca[b], Stanislav Gordeyev[b], and Eric Jumper[b]

[a]MZA Associates Corporation., 1360 Technology Ct. Suite 200, Dayton, OH, USA 45430
[b]University of Notre Dame, Notre Dame, IN, USA 46556

ABSTRACT

We present our findings from a modeling and simulation effort in which we analyzed the imaging performance of a turreted laser beam director/telescope on a transonic aircraft platform. We used real wavefront sensor (WFS) data collected by the Airborne Aero-Optics Laboratory-Transonic (AAOL-T) test platform at Mach 0.8. Using these WFS data, we quantified the imaging point spread function (PSF) for a variety of line-of-sight (LOS) angles. The LOS angle values sweep from forward-looking angles, through the shock wave to backward-looking angles, imaging through the turbulent wake. Our simulation results show Strehl ratios from 4% to 50% with substantial scattering of energy out to many times larger than the diffraction-limited core. For each LOS angle, we analyzed the imaging modulation transfer function (MTF) which showed a rapid reduction of contrast for low-to-mid range spatial frequencies. We reaffirm that practical limits to usable spatial frequencies require higher imaging signal to noise ratio in the presence of aero-optical disturbances at high Mach number. The presented MTF analysis speaks to the degradation of image-contrast-based tracking algorithms that rely on an illuminator laser propagating through aero-optical aberrations. In conclusion, we discuss the AAOL-T imaging flight test campaigns and the anticipated imaging performance of AAOL-T turret.

Keywords: aero-optics, imaging, image resolution, point spread function, modulation transfer function, airborne systems

1 INTRODUCTION

The acquisition, tracking, and pointing (ATP) function for a laser system must generally look through the same optical/mechanial system being used as a beam director or turret on an aircraft platform.[1] The aerodynamic environment of the laser turret imparts both mechanical jitter and optical aberrations into the path of sensors being used for ATP functionality.[2] Aero-optical effects around a directed energy turret are optical distortions imposed on a propagating laser beam due to a varying density field around an aircraft, as the density field affects the local index-of-refraction.[3–5] The density variations are caused by either compressibility effects at flight Mach numbers above 0.2 or by pressure variations. In this sense, the physical cause of aero-optical effects is different from atmospheric optical effects, which are caused by total temperature variations in the atmosphere. At transonic speeds, an unsteady, turbulent, shock structure will develop about the turret, producing large variations in entropy, unsteady, separated flow regions and resulting large density and an index of refraction gradients that will defocus and scatter the beam.[6]

An outgoing laser beam will get distorted by fast-moving and spatially-varying aero-optical effects, resulting in a larger than diffraction-limited laser spot and, as a consequence, a lesser intensity on a target. Likewise, an image of a distant object will be distorted by these aero-optical effects created by the turbulent flow features formed around the aircraft and, specifically, around the turret. Thus, aero-optical effects even in the absence of atmospheric optical effects will degrade the performance of an otherwise high-resolution imaging system, similar to a degradation of a beam focusability in the far-field in case of directed energy or communication systems.

Send correspondence to Yakov Diskin
E-mail: Yakov.Diskin@mza.com
Phone: (937) 684-4100 x120

Laser Communication and Propagation through the Atmosphere and Oceans VI, edited by Jeremy P. Bos, Alexander M. J. van Eijk, Stephen M. Hammel, Proc. of SPIE Vol. 10408, 104080N · © 2017 SPIE
CCC code: 0277-786X/17/$18 · doi: 10.1117/12.2275648

In this paper, we quantify the contrast and resolution reduction caused by aero-optical aberrations on imaging systems. In Section 2, using high-speed WFS data, our modeling and simulation work shows that a modulation transfer function (MTF) can be computed and provides a measurable quantity of the aero-optic imaging degradation. Furthermore, in Section 3, a validation experiment is presented in which the wavefront MTF simulations are compared to contrast MTFs computed from resolution charts. In Section 4, we describe the ground and flight imaging experiments as well as the setup of the Airborne Aero-Optics Laboratory-Transonic (AAOL-T), an aircraft laboratory capably operated by the University of Notre Dame (UND). We describe the MTF processing algorithm and the associated results. The algorithmic steps account for the numerous lessons and adjustments need for real flight image data MTF processing. Our analysis concludes with a list of important lessons learned for future aero-optic imaging flight campaigns. In Section 5, we conclude our findings and discuss future work. A companion paper[7] provides additional description of the flight tests and detailed analysis of effects of aero-optical distortions on image quality.

2 AERO-OPTIC IMAGING DEGRADATION MEASUREMENTS USING WAVEFRONT DATA

The aircraft wavefront data used for these studies was obtained from the AAOL-T[4,8] test platform operated by UND. The AAOL-T is a five-year multidisciplinary research program sponsored by the High Energy Laser Joint Technology Office to address transonic aero-optics measurements and mitigation through theory, simulation, wind-tunnel testing, and airborne field tests. The AAOL-T consists of two aircraft flying in close formation with a 50m separation. One of the aircraft, the source aircraft, projects a diverging $\lambda = 532nm$ laser beam onto the other aircraft, called the laboratory aircraft, shown in Figure 1. The hemispherical turret is $D_t = 0.3048m$ (12-inch) in diameter and is installed on the laboratory aircraft with a turret base height of $h_t = 0$. The turret has a conformal window[9] aperture of $D_{ap} = 0.1016m$ (4-inch) in diameter. Both the incoming laser beam and the turret actively track each other using independent point-and-tracking systems, so the incoming laser beam is always at the turret aperture and the turret always faces the incoming laser beam; a detailed description of the tracking systems and the optical layout of the turret are provided in Jumper *et al.*[4] Figure 1 shows photographs of the AAOL-T hardware during tests conducted on the program.[6]

(a) (b)

Figure 1. Photographs of AAOL-T hardware during testing. (a) The sensor turret integrated on the aircraft receiving the green test beam in flight. (b) A closer look at the AAOL-T turret integrated on laboratory aircraft.

For these tests, wavefronts were collected using high-speed Shack-Hartman WFS operating at a 20 kHz sample rate with 30 subapertures across spanning the aperture, D_{ap}.[10,11] Wavefront data sequences were collected at several different turret azimuth and elevation angles spanning a range of turret-window viewing angles. Figure 2(a) shows the turret pointing angles with respect to the flow direction. The azimuth and elevation angles are designated α and β, respectively. The line-of-sight angle (LOSangle), γ, is calculated from the azimuth and elevation angles by

$$cos\,\alpha = cos\,\beta\,cos\,\gamma. \tag{1}$$

Figure 2(b) shows a time history of wavefront measurements. The flow direction in these wavefronts is from upper left to lower right. We note the presence of wavefront structures that flow through the aperture, but are not

completely "frozen" with the flow. Instead, there is an evolution of the wavefront features as they traverse the aperture.

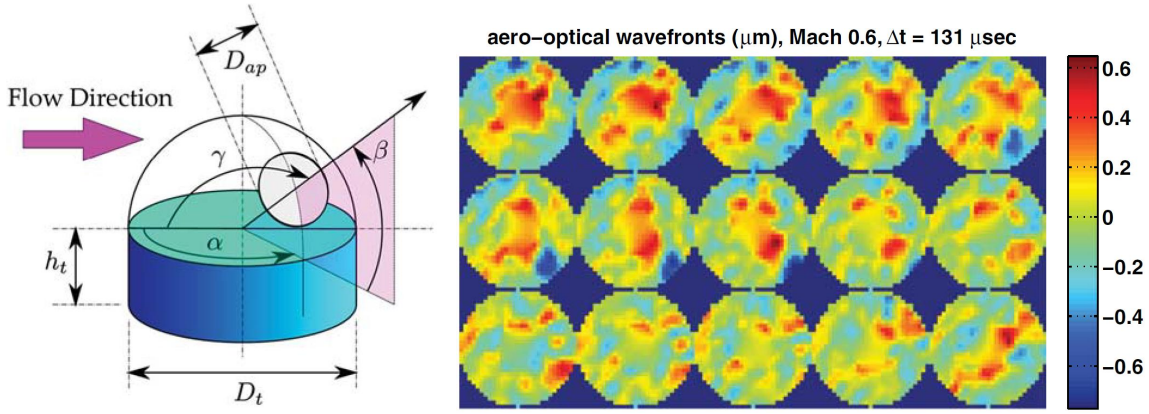

(a) (b)

Figure 2. (a) Turret pointing angles with respect to flow direction. α is the azimuth angle. β is the elevation angle. γ is the window angle. D_t is the turret diameter. D_{ap} is the aperture diameter. h_t is the turret base height. (b) Time history for wavefronts at turret view angle. Time evolution is across each row with $\Delta t = 131\mu s$

The AAOL-T flight wavefront measurements at Mach 0.8 were used to simulate the imaging properties of an aircraft turret system working at 30-kft altitude for the platform. We used real wavefront time histories with 20,000 samples collected at 20 kHz frame rate on the WFS. We compute the point spread function (PSF)[6,12] for each wavefront with imaging $\lambda = 532nm$ and $D_{ap} = 0.1016m$. These PSFs were averaged over the wavefront sequence to evaluate the average optical performance of a system. Figure 3 shows the simulated PSF for LOSangles 89°, 98°, 113°, 125°, and 136° (LOSangle 148° was computed, but is not shown due to space considerations. The 148° PSF is similar to the 136° PSF.). These PSFs are compared with the diffraction-limited PSF in Figure 3(a). The equivalent peak Strehl ratio, S_{aero}, is computed by normalizing the peak intensity of each PSF by the peak of the diffraction-limited performance. A notable characteristic of the aero-optics PSFs with changing LOSangle is the greater scattering of energy at the look-back angles (110° to 150°), far beyond the diffraction-limited central core.

To quantify the aero-optical effect on imaging, we computed metrics for the PSF. Figure 4 is taken from Morrida *et al*[13] and shows the trends of OPD_{RMS} error as a function of LOSangles. The trends are inversely correlated to the computed peak Strehl ratios.[14] We overlaid the plot with computed peak Strehl ratios for the selected test angles, marked by yellow stars. As seen in the PSFs in Figure 3, the look-back angles demonstrate a wide-angle scattering that causes a rapid drop in the peak Strehl ratio. Thus, we expect the resolving power of the optical system to be significantly impacted by these look-back angle disturbances.

The contrast-reduction characteristic of aero-optical disturbances on imagery from the aircraft platform can be quantified by considering the MTF of the optical system including aero-optical disturbances. For each of the PSFs shown in Figure 3, the MTF was computed as the modulus of the optical transfer function (OTF) $H(k_x, k_y)$. The OTF is simply the Fourier transform of the PSF,[15] $h(k_x, k_y)$. The MTF can expressed as follows,

$$MTF(k_x, k_y) = |H(k_x, k_y)| = |F\{h(x, y)\}|. \tag{2}$$

The OTF for the diffraction-limited vacuum case is shown in Figure 5(a). The MTF for each LOSangle considered is shown in Figure 5(b). To present these data, we have radially averaged the OTF in the spatial-frequency plane, and normalized the scalar spatial frequency k to the cut-off frequency of the optical system, $D_{ap}/\lambda L$. The yellow rings in Figure 5(a) illustrate the angularly averaging concept. When presented in this manner, we clearly see the influence of aero-optical disturbances with changing LOSangle. As the turret points back we see the lower spatial frequencies are severely attenuated in the imaging system. Since the MTF quantifies the

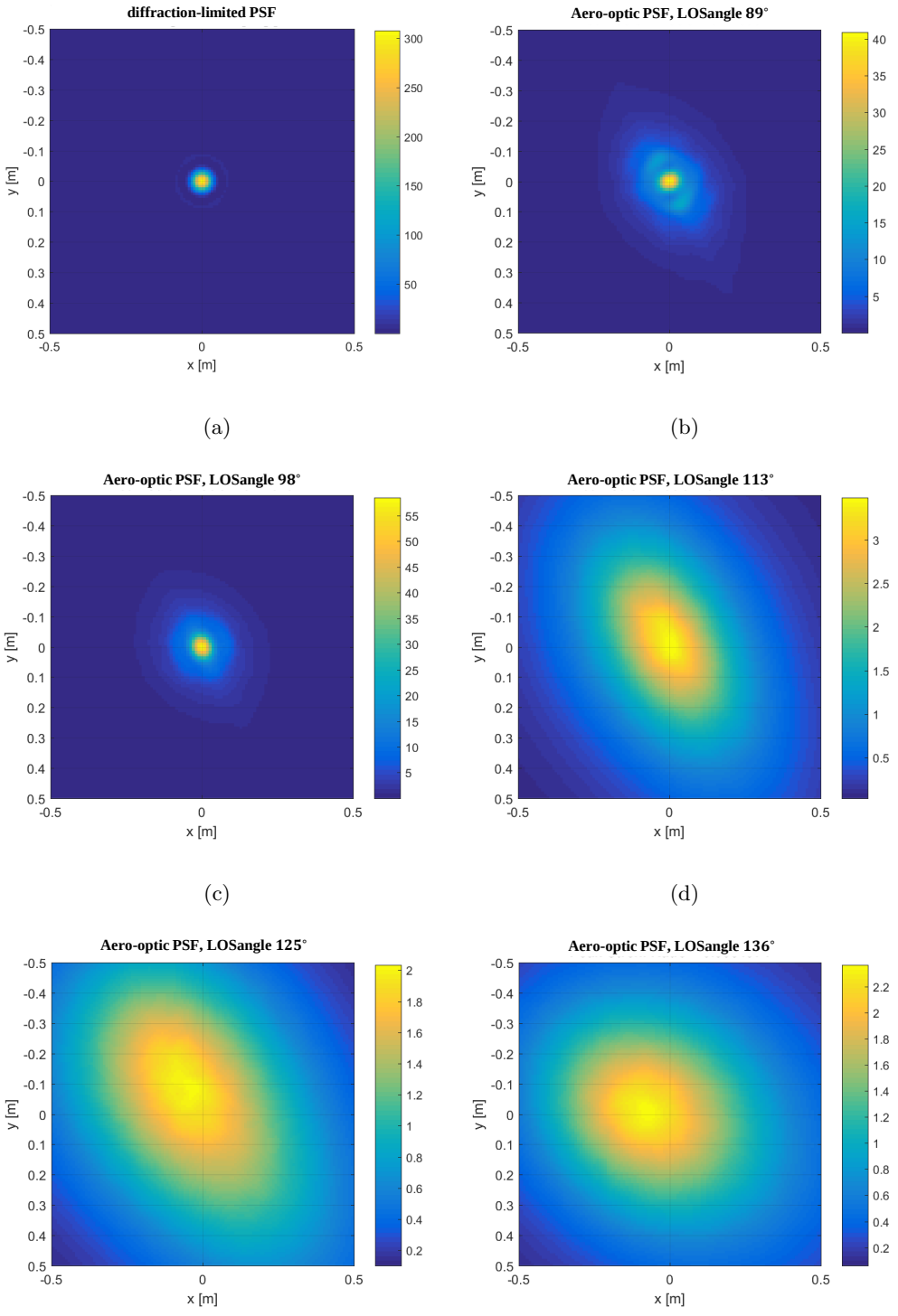

Figure 3. Imaging PSFs including measured aero-optical disturbances. (a) Diffraction-limited PSF. (b)-(f) PSF with aero-optical disturbances at LOSangle 89°, 98°, 113°, 125°, and 136°, respectively.

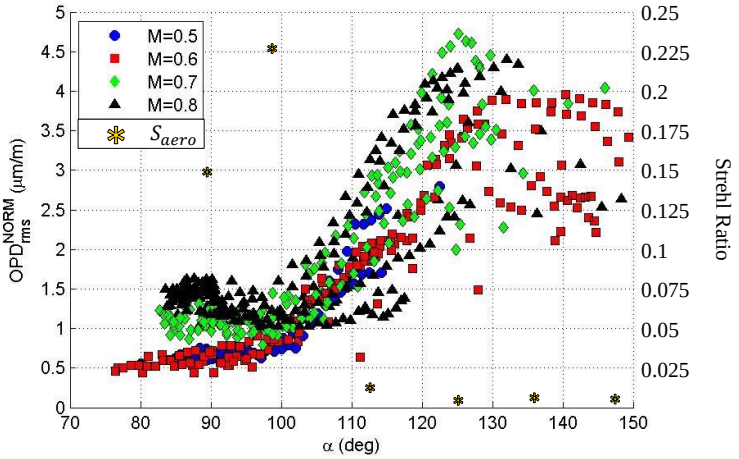

Figure 4. Morrida[13] depicts the trends of the normalized OPD_{RMS} versus viewing angle for a hemispherical turret as measured on the AAOL-T for various Mach numbers. The peak Strehl ratio (S_{aero}) using the PSF averaged at Mach 0.8 for the selected angles is plotted in yellow

contrast of sine waves at each spatial frequency, the reduction of the MTF with increasing LOSangle shows that a major effect of aero-optical disturbances on imaging is the reduction of the contrast in the image. Reduction in contrast represents the loss of higher frequency details in the image. When we consider an arbitrary limit where the MTF is 10% of its peak (indicated by the dashed line in Figure 5(b)) the spatial frequency at which each MTF line falls below this value may be thought of as the effective reduction in resolution of the system. Given this interpretation, we see that for LOSangles 89° and 98° the imaging resolution is approximately 70% of diffraction-limit. The resolution falls below 30% at LOSangle 113°. For LOSangle 125°, 136°, and 148°, the resolution is less than 20% of diffraction-limit, i.e. the smallest object that can be resolved by the system looking aft is 5× larger than the smallest resolvable object at diffraction limit.

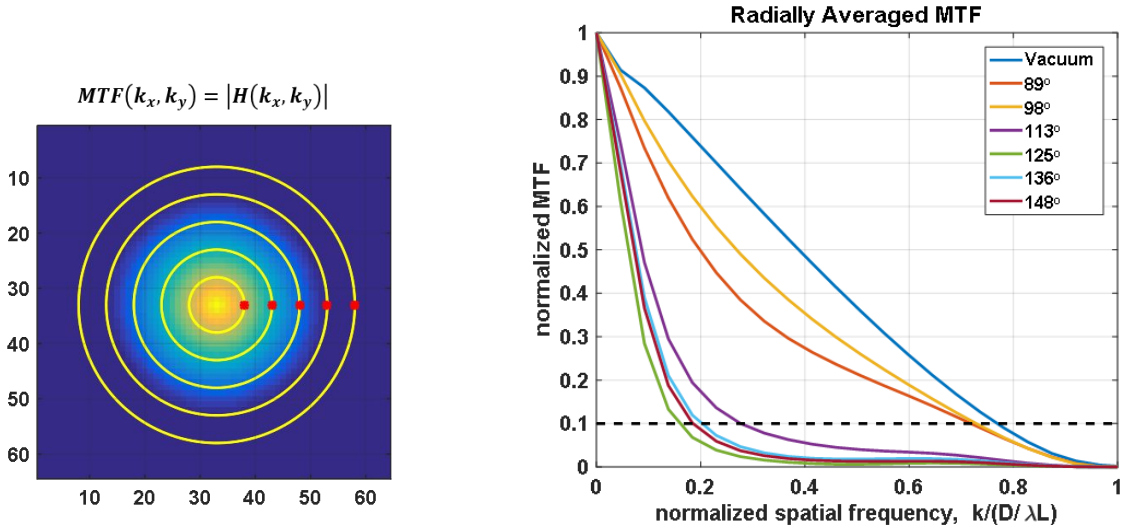

(a) (b)

Figure 5. (a) The OTF is computed by taking the Fourier transform of the PSF. The OTF of the diffraction-limited case is illustrated. Angularly averaged rings allows us to form a 1D representation of the OTF/MTF. (b) Normalized modulation transfer function (MTF) for imaging with aero-optics.

3 VALIDATING WAVEFRONT DATA MTF AGAINST COMPUTED IMAGE MTF

The modulation transfer functions (MTFs) described in the previous section are Fourier optics simulations based on measured wavefront sensor data. In order validate those simulations, we conducted a series of experiments in which we computed the MTF for a captured image. A MTF curve represents the spatial frequency response of the imaging system. The measured response is the percent contrast quantifiable at various spatial frequencies. To compute a contrast percentage at a specific spatial frequency, we must evaluate a modulating - black and white - element.[15] Using alternating black and white lines of a specified spatial frequency or width, we can quantify the contrast percentage as follows,

$$\%\, contrast = MTF = \left(\frac{I_{max} - I_{min}}{I_{max} + I_{min}} \right). \tag{3}$$

I_{max} and I_{min} represent the maximum and minimum intensities for the considered spatial frequency element. Theoretically, only two pixel values are needed to compute a MTF. However, to make the computation statistically reliable more pixels are recommended.[16] We used three-line-element sets to compute MTF points.

The validation experiment utilized a pristine resolution image. With a pristine image, the MTF contrast is 100% for all spatial frequencies. The image dimensions must be large enough to avoid pixelization artifacts in the MTF computation. Thus, the smallest spatial element must contains several pixels in the width of a single white or black line. We set our pristine image dimensions to 1028×1028. Next, we convolve the pristine image with the PSFs associated with the aero-optic disturbances at various LOSangles. In Figure 6(a) and 6(b), we used the PSFs from Figure 3 to simulate the blurring that would occur at LOSangle of 89° and 125°, respectively. Those angles were selected as representative of a forward-looking angle, 89°, that has minor aero-optical distortions and a backward-looking angle, 125°, with significant aero-optical effects. From Figure 6, we can visualize the blurring impact of strong aero-optical distortions.

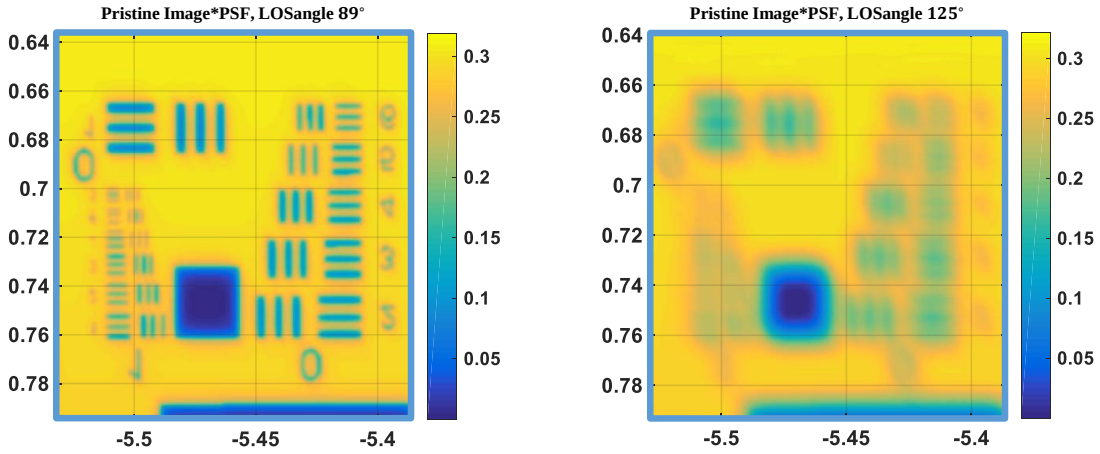

(a) (b)

Figure 6. A pristine image containing a variety of spatial frequency elements is convolved with a PSF from wavefront data. (a) 89° is a forward-looking angle with tighter SPF spot,(b) 125° is a backward-looking angle experience a wider spread due to significant aero-optical distortions.

We referred to USAF-1951 resolution target board, shown in Figure 7(a), as a guide for determining spatial element sizing. The red bounding boxes enclose the selected processing regions. The target board consists of four groups. Each group consists of six elements, numbered from 1 to 6. The target board resolution is measured in line pairs per millimeter (lp/mm) and computed by the following expression.

$$Resolution(lp/mm) = 2^{Group + (Element-1)/6} \tag{4}$$

Each element has a vertical and horizontal set of lines. Thus, two separate MTF curves can be computed using only vertical and only horizonal element lines. In Figure 7(b), we convolve the pristine image with the diffraction-limited PSF (vacuum) and compute the MTF directly from the blurred image of the resolution chart. The vertical elements in red and horizontal elements in blue produce a similar MTF curve. The most significant deviations occur in the high spatial frequency elements, where the lines are thin and pixelization artifacts influence the contrast scoring. In Figure 7(c), we average the vertical and horizonal MTF scores to form a combined 'computed' vacuum MTF, shown with blue stars. The MTFs simulated using wavefront data (Fourier transform of PSF) are shown in solid lines. Comparing the computed MTF scores from the blurred image to the simulated MTF curves from the radially averaged OTF, we note strong consistency between the two techniques. In the case of strong aero-optics, shown in purple, we observe the curve crossing the 10% noise level at 0.18 of diffraction-limited spatial frequency. We observed similar correspondence between the computed versus simulated MTF for all tested LOSangles. Small differences between the computed and simulated are visible, and are likely caused by the discrete nature of the pixels and averaging steps (horizontal and vertical MTFs) in the computation process. We considered these differences insignificant and the algorithm for computing the MTF curves from images validated.

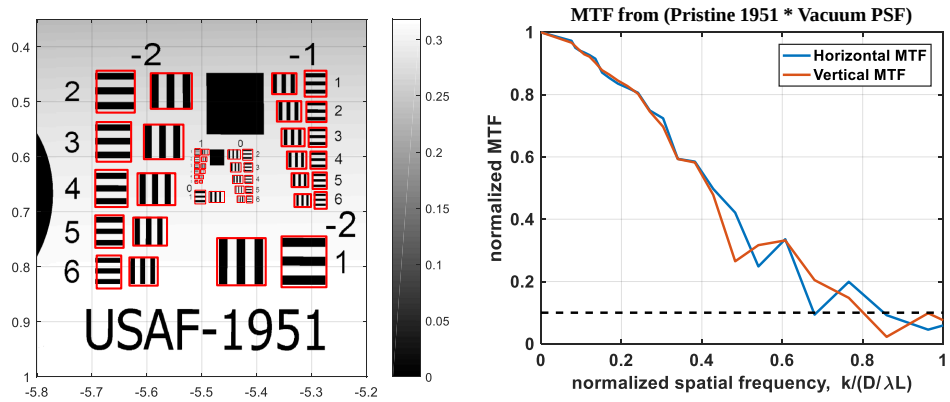

(a) (b)

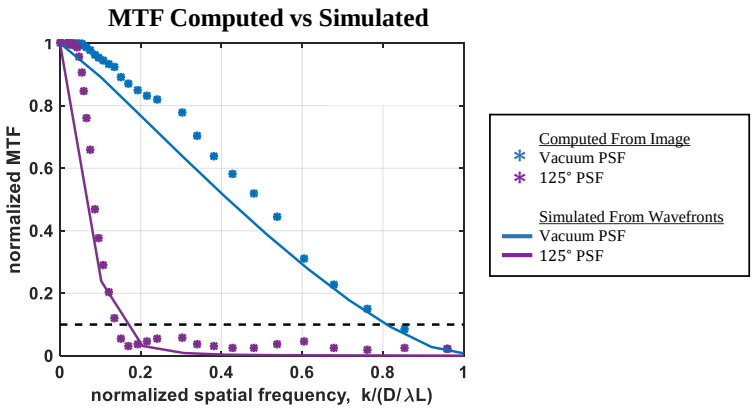

(c)

Figure 7. (a) The USAF-1951 resolution target board used as the pristine image. The red bounding box indicated the areas selected for processing each resolution element. (b) The pristine image is convolved with the diffraction-limited PSF. The plot compares the MTFs produced the horizonal and vertical three line element sets. (c) Comparing the MTFs produced by computing percent contrast from a blurred image with the simulated MTFs from the wavefront data. The MTFs for the vacuum case and LOSangle 125° are illustrated.

4 EXPERIMENTAL RESULTS AND ANALYSIS

We report on three different imaging experiments using the AAOL-T turret. Each experiment builds on the conclusions of the prior tests. The first is an indoor ground test designed to evaluate the optical performance of the turret. The second test is a flight campaign in October 2016 that utilized the three-line element sets to measure aero-optical distortions. The third experiment is a secondary flight campaign flown in May 2017. The following subsections describe each experiment and conclusions drawn from the data.

4.1 Experiment 1: Indoor Imaging Through Turret

The first set of experiments is designed to be a performance marker and set the expectations for image quality during flight tests. The two main objectives are 1) to evaluate the optical precision and imaging capabilities of the AAOL-T turret and 2) to determine whether a teleconverter enhances the imaging performance. For this experiment, the turret is placed indoors at $L = 50.9$m from to a USAF-1951 resolution target board. The board consists of four groups with each containing six elements. Several spotlights are placed at the target board to illuminate the resolution pattern.

To determine the optical imaging capabilities of the AAOL-T turret, we capture imagery of two USAF-1951 boards. One target board, referred to as 'Large', contains larger spatial elements spanning from 3% to 35% of diffraction limit. The second target board is smaller, referred to as 'Small', and therefore contains higher spatial frequecies spanning from 8% to 100% of diffraction limit. The smaller board allows us to compute values across the full diffraction limit range, however all the smaller targetboard elements are within the 10% noise level. On the other hand, the large target provides several measurable elements that allows us to make conclusions on imaging performance.

Since the turret is indoors and stationary, the images captured contain no aero-optical distortion. In this experiment, when the turret captured an image the degradation is purely due to the optical precision of the turret and camera detector. Figure 8(a) illustrates the image captured by the turret under these 'No Aero Optics' or vacuum-like conditions. The images are collected using the Phantom v1611 camera. The lens for the imaging camera had an adjustable focal length from 150-500 mm with a minimum f-stop of 8.

Additionally, we evaluate the benefits of using a 2x teleconverter attached to the lens to double the effective focal length. For the actual images, the lens was set to a focal length of 300 mm, giving an effective focal length of 600 mm, and the f-stop was set to the minimum value of 8 to maximize the incoming light. Without using the 2x teleconverter (no doubler),the instantaneous field-of-view (IFOV) is 10.6 μrad which is $2.03(\lambda/D_{ap})$. The signal-to-noise ratio (SNR) is 41.7. We define "resolution" as the largest element where line pairs cannot be distinguished. Based on that, the smallest visually resolvable element on the large USAF-1951 resolution target board is Group 1 Element 2, representative of 2.7mm line pairs. With the 2x teleconverter (doubler), the IFOV decreases to 5.7 μrad which is $1.09(\lambda/D_{ap})$, representative of 0.3mm line pairs. With the doubler the SNR is reduced to 10.3, and the smallest resolvable element on the resolution target board is Group 1 Element 1. Directly comparing the resolution capabilities, the doubler resolves $5.7(\lambda/D_{ap})$ while no doubler resolves $5.1(\lambda/D_{ap})$. In Figure 8(b), we show the MTF performance on the two different scales of target boards as well as with and without the 2x teleconverter. We referred to the usage of the 2x teleconverter as 'With Doubler' and performance without the teleconverter as 'No Doubler'. The plot shows all four MTFs representing the vacuum 'No Aero Optics' case. Small differences between the four MTF curves are a result of varying SNR, IFOV, and pixelization artifacts. values The MTF curves are significantly degraded when compared to perviously computed vacuum MTFs in Figure 7(c). The MTF curves in Figure 8(b) reach the 10% noise line to the left of 20% diffraction limit. In other words, the ideal no aero-optics case produces MTFs on par with the simulated strongest aero optical distortions of the look-back angles.

In Figure 8(c), we convolve the PSF from a severe aero-optic LOSangle 125° with the captured image in Figure 8(a). As a result, the visible noise of the no aero optics case is eliminated and the resultant image appears cleaner. However, the convolved PSF also blurs the small spatial frequencies and thus reduces the percent contrast. When visually comparing the curves in Figure 8(b) to those in Figure 8(d), very little difference is noticeable. The MTF reached the 10% noise line at 18% in Figure 8(b), while in Figure 8(b) the noise line is crossed at 11% of diffraction limit. From these plots, we can conclude that the predominant image distortions are due to the quality

of the optics within the turret. The aero-optic effect is small and the computed MTF plots have low sensitivity to those distortion.

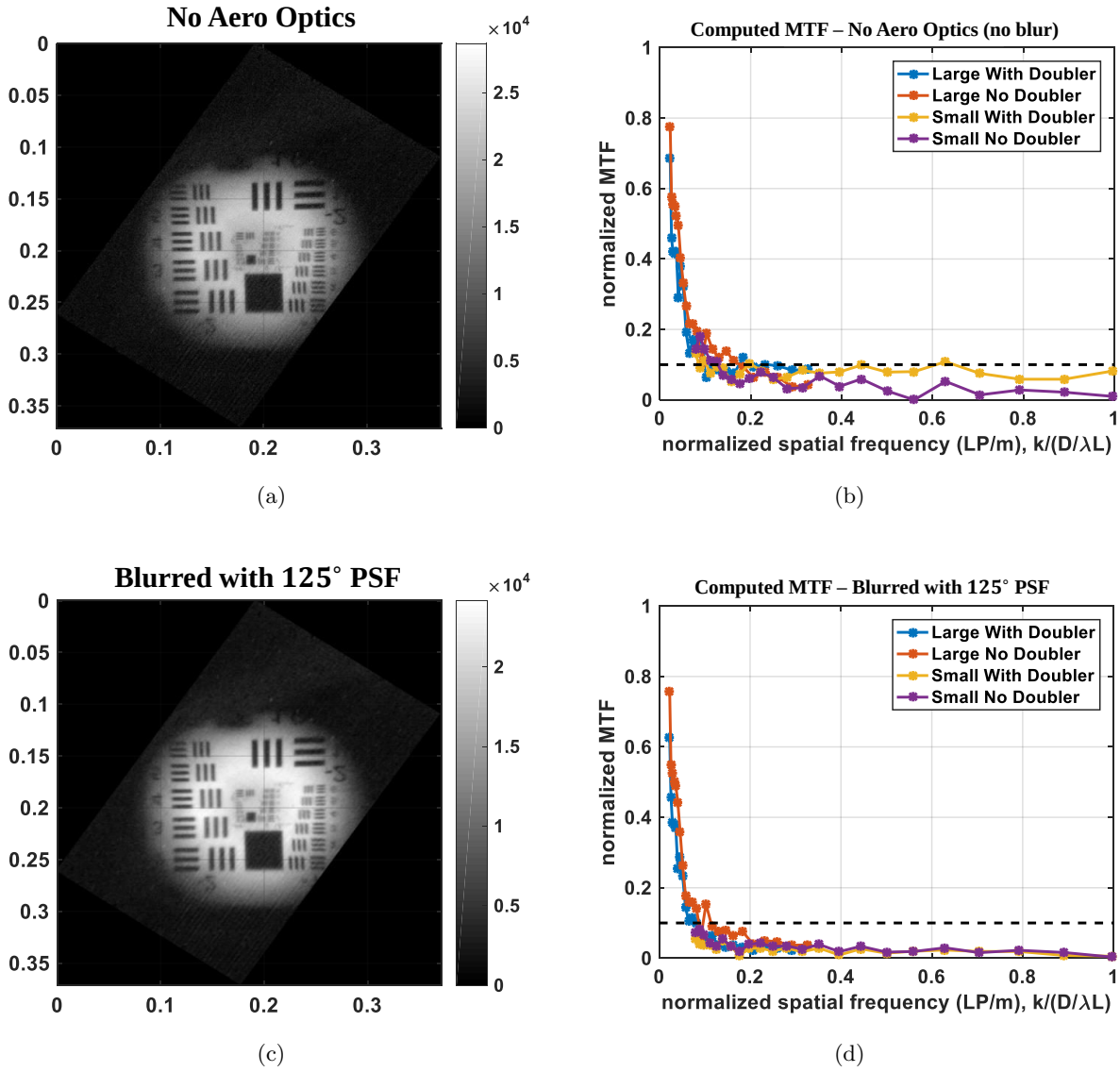

Figure 8. (a)An image of the 'Large' target board captured via AAOL-T turret indoors. Since the image is taken indoors there are no aero-optical effects, thus this image is referenced as the 'No Aero' cases. (b) MTFs for the 'No Aero' cases computed on the large and small target boards, as well as with and without a doubler. (c) The captured image is convolved with the PSF of LOSangle 125°. This LOSangle contains significant aero-optical effects. (d) MTFs from the convolved image computed on the large and small target boards, as well as with and without a doubler.

In order for us to evaluate the pure aero-optical degradation, we proposed dividing out the optical MTF distortions. Thus, the aero-optics MTF can be computed as,

$$Aero\,MTF = \frac{Simulated\,MTF}{Vaccum\,MTF} = \frac{Blurred\,Target\,MTF}{NoAero\,MTF} \tag{5}$$

where the $Simulated\,MTF$ is produced by evaluating the wavefront data associated with a flight LOSangle, and the $Vacuum\,MTF$ is the diffraction limited case. Equivalently, when computing the MTFs from captured

imagery, the *Blurred Target MTF* is the captured image containing all the distortions (aero-optical, imperfect lens optics, etc). The *NoAero MTF* is the indoor ground image that contains all camera and optics distortions but no aero-optical degradation.

In Figure 9, we plot the *Aero MTF* computed from the wavefront simulations, pristine image processing, and imaging with the AAOL-T turret. We present the *Aero MTF* results for a side-looking LOSangle of 98° with minor aero-optical degradation in Figure 9(a). In Figure 9(b), we present the results of a backward-looking LOSangle of 125° containing significant aero-optical disturbances. In each plot, the solid green line represents the theoretical wavefront simulation result wherein we divided the MTF of the LOSangle by the MTF of vacuum case. The curves of the wavefront simulation MTFs and associated calculations are described in Section 2. Next, the pristine image processing computations are labeled as 'AF1951 Sim' and marked with a solid purple starred line. For this *Aero MTF* we used a pristine image of the USAF-1951 resolution target board convolved with a degraded LOSangle PSF and divided by the same pristine image convolved with a diffraction-limited vacuum PSF. The difference between the green and starred purple line is representative of MTF processing error associated with pixelization artifacts at high and low spatial frequencies. At high spatial frequencies in the pristine image, pixelization artifacts cause the fine line elements to vary in width. For example, spatial element associated with $0.8(\lambda/D_{ap})$ will have one black line with a 2 pixel width and another black line with a 3 pixel width. When these lines are blurred with a PSF the width of the lines impacts the MTF calculations. Similarly, for the low spatial frequencies the radially averaged OTF approach is limited by a minimum radius size. Therefore, values between 0 and 0.05 of (λ/D_{ap}) are linearly estimated for the solid green theoretical line. Additionally, Figure 9 shows the *Aero MTF*s computed by using the images captured through the AAOL-T turret. Blue stars show the performance with the 2x teleconverter (With Doubler) and red star show the performance without the 2x teleconverter (No Doubler).

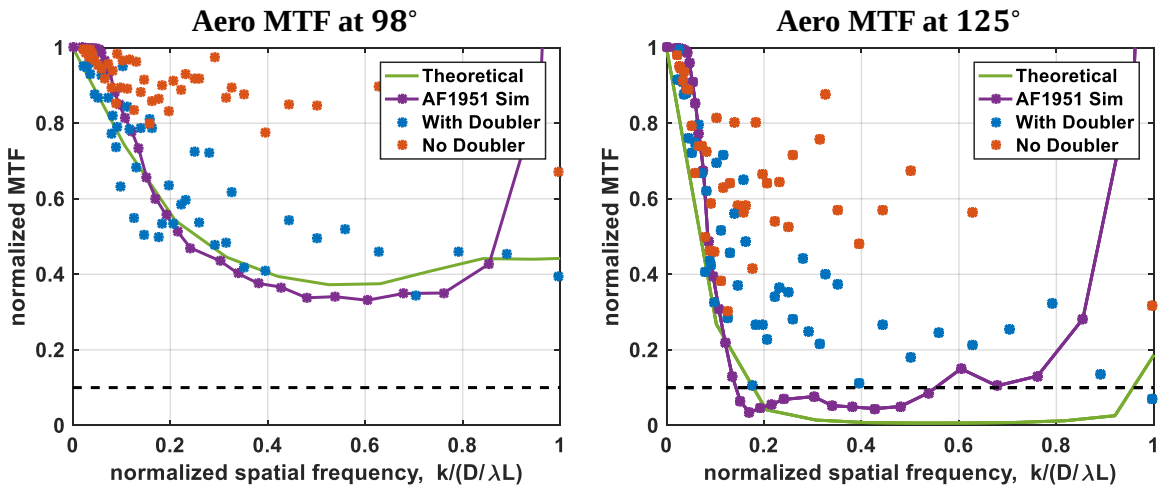

(a) (b)

Figure 9. Computing the Aero MTF using: 1) wavefront simulations (Theoretical), 2) pristine USAF-1951 resolution target board blurred with PSFs, 3) imaging a resolution target board through the AAOL-T turret with the 2x teleconverter, 4) imaging through the AAOL-T turret without the 2x teleconverter. (a) Using the lower aero-optic distortion case of forward looking LOSangle 98°. (b) Significant aero-optic distortion at the backward-looking LOSangle of 125°.

By analyzing Figure 9(a) and Figure 9(b), we are able to make certain conclusions on the impact of aero-optical disturbances on the imaging MTFs and the overall imaging capabilities of the AAOL-T turret. The LOSangle 98° case shows the normalized MTF rapidly decreasing with from 0 to 0.4 of (λ/D_{ap}) after which the *Aero MTF* levels off and remains at $\tilde{4}0\%$ contrast. The ratio between the LOSangle 98° MTF and the diffraction-limited vacuum cases remains the same from 0.4 to 1 of (λ/D_{ap}). In other words, for those spatial frequencies the

distortion rate is the same as the diffraction limited vacuum case. The measurable degradation occurs between 0 and 0.4 of (λ/D_{ap}). Similarly, for the LOSangle 125° case, we observe a sharp drop off in the low special frequencies and the *Aero MTF* leveling off after 0.16 of (λ/D_{ap}). Therefore, the *Aero MTF* region of interest (ROI) are the spatial frequencies in which the LOSangle distortion decreases quicker than the diffraction limited vacuum case. Additionally, Figure 9 shows that the performance with 2x teleconverter (With Doubler) more closely aligns with the wavefront theoretical curves. Based on this analysis, we elected to use the doubler in the flight campaigns.

4.2 Experiment 2: Flight Campaign with Resolution Elements

The indoor imaging experiment also proved useful in designing a target board that allows us to compute an MTF from flight tests. The first imaging AAOL-T flight campaign flew in October 2016 out of Grand Rapids, MI. To perform in-flight measurements of image degradation due to aero-optical effects, a target board, shown in Figure 10(a), was placed around the window of the laser aircraft. The target board consisted of a collection of three-line-elements of various resolution. We followed the precise line pairs per meter spacing of the original USAF-1951 target board. Due to the narrow FOV, our flight formation consisted of a $L = 150m$ separation between the two aircraft, so the target board resolution elements extended to groups -3, -4, -5, and -6. Each element consisted of a vertical and horizonal 3 line set. The elements were positioned to optimize the space around the airplane window. Figure 10(b) illustrates the distribution of the target board elements on the normalized MTF plot. The plot shows that Group 0 Element 2 (where the width of a single black line is 0.45mm) is the last element theoretically resolvable before diffraction limit at $L = 150m$. The largest element on the target board is Group -6 Element 6, where the width of a single black line is 17.9mm. Interestingly, Figure 10(b) show that the elements we expected to visually see modulate are all clustered in the low spatial frequencies. Thus, 19 MTF points are positioned between 0 amd 0.18 of (λ/D_{ap}), while 14 MTF points populated between 0.2 and 1.0 of (λ/D_{ap}).

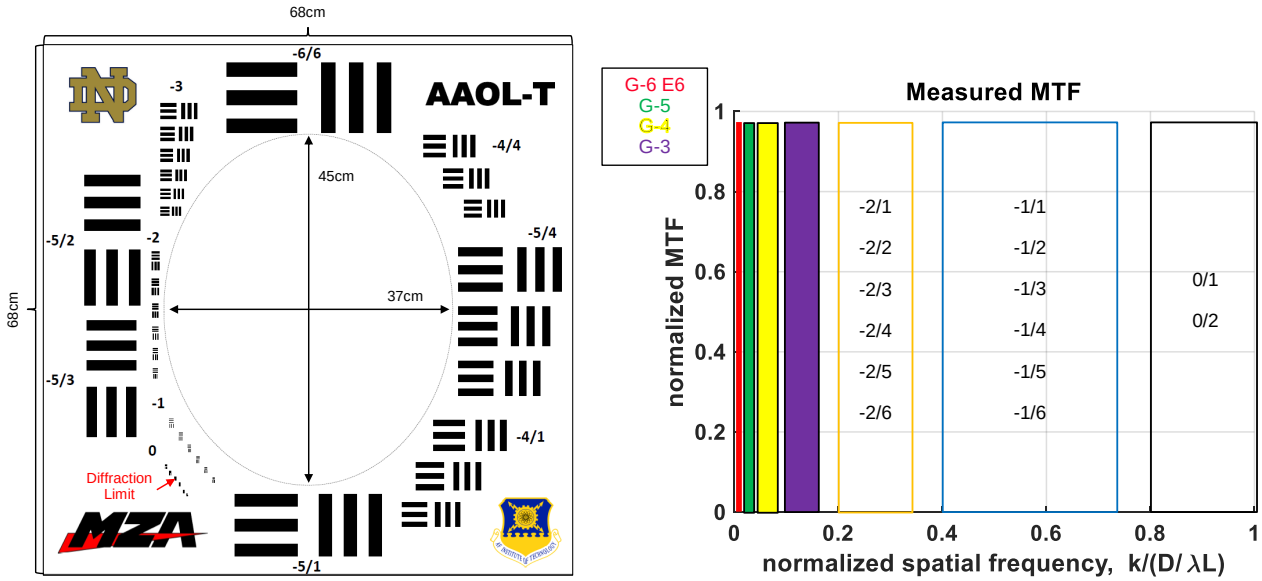

(a) (b)

Figure 10. (a) Resolution target board design positioned around the window of the laser aircraft. Resolution elements span from Group 0 Element 2 to Group 6 Element 6 according to the original USAF-1951 resolution target board. (b) The design groups and elements represent 33 MTF points which sparsely cover the normalized spatial frequencies to diffraction limit.

The campaign consisted of four flights with 80 data points. An example of three data points is shown in Figure 11. Figure 11(a) shows an imagery sequence captured on the ground. This sequence represents the 'no aero optics'

case that will be use as the baseline for extracting the *Aero MTF*. We note that in this "clean" case, we observe a vignetting effect that partially dims significant portions of the target board. The largest three-line-elements are clearly distinguishable, however the visual modulation is lost within the elements of Group -3. We can make out the location of Group -2 elements, but unable to see modulation. Groups 0 and -1 are not visible in the ground – No Aero – image.

Figure 11(b) and Figure 11(c) illustrate effects of two turret operation modes: "Coarse Tracking" and "Fine Tracking". In the "Coarse Tracking" operational mode, the turret is physically pointed at the source laser using a sidecar camera located on the turret ball in a low frequency feedback control loop. In the "Fine Tracking" operation mode, the jitter on the incoming laser after having passed through the turret is mitigated using a fast-steering-mirror (FSM) and a position sensing device (PSD) in a high frequency feedback control loop. Because the integration time of the imaging camera is relatively long, the residual jitter on the beam results in blurring of the image. When "Fine Tracking" is engaged, the residual jitter is significantly reduced compared to "Coarse Tracking" and less image blurring due to jitter should occur.

Both in-flight illustrations experience significant blur, however our reached a consensus is that the "Fine Tracking" turret operation mode tends to be slightly clearer than "Coarse Tracking" mode. Figure 11(b) illustrates an in-flight sequence from look-back LOSangle 142°. This LOSangle contains significant aero-optical distortions that almost completely blur all the target resolution element. The largest two elements, Group -6 Element 6 and Group -5 Element 1, have some visible modulation while the rest of the elements do not appear resolvable. Figure 11(c) depicts an image from an in-flight sequence as well. The LOSangle 114° contains moderate aero-optical distortions. This image is captured using the "Fine Tracking" turret operation mode. We observe that the LOSangle 114° image contains more blur than the ground case but less than the LOSangle 142° case. We note that the distortions do not seem to be consistent across the aperture. Larger elements, Group -5 Element 2 and Element 3, are not visible at all while slightly smaller elements, Group -5 Element 5 and Element 6, are distinguishable and quantifiable. Overall, the vignetting partially or completely dimmed the majority of the resolution elements and proved to be a significant hurdle in the MTF processing.

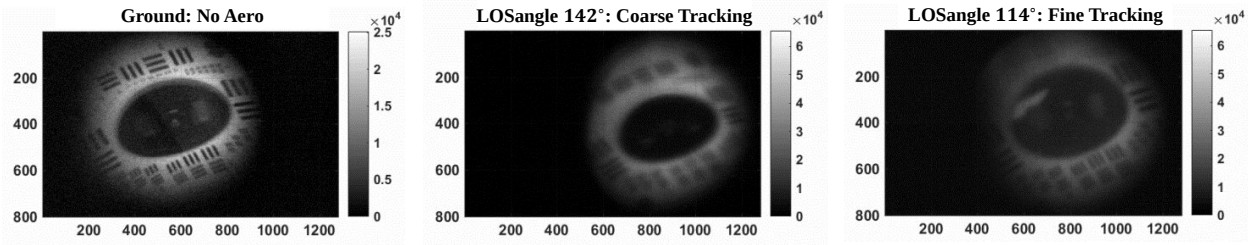

(a) (b) (c)

Figure 11. AAOL-T imaging turret capturing frame sequences at $L = 150m$. (a) Ground baseline imagery that contains no aero-optically distortions. (b) Flight data of LOSangle 142° using the coarse tracking mode. (c) Flight data of LOSangle 114° using the fine tracking camera mode.

The poor imaging results in uncertainty within the MTF computation. We applied processing to neutralize the vignetting and normalized the contrast scoring across the image. Additionally, the images must be rotated to form vertical and horizonal elements. The rotation is dependent on the LOSangle. Therefore, for each collection the corrective rotation is slightly different. Rotating images introduces additional blurring due to interpolation artifacts. In Figure 12(a), we show the MTFs computed from the three images in Figure 11. In blue, labelled as "No Flow", the ground case with no aero-optical distortion is computed. We presented the data on a logarithmic x-axis plot because the ROI is within the largest spatial frequencies starting with 0.2 of (λ/D_{ap}). In red, labelled as "Fine Track", is the LOSangle 114° captured in the fine track camera mode.[17] Finally, in orange and labelled as "Coarse Track", is the LOSangle 142° captured in coarse tracking mode.[17] In all three images high frequencies elements (0.2 to 1.0 of (λ/D_{ap})) are not visible and the MTF algorithm is unable initial the area to compute a contrast score. Spatial frequencies without a computed MTF score are marked with zeros. For the larger

resolution elements, we note that the "No Flow" case has the highest MTF contrast scores, as expected. The "Fine Track" slightly outperforms the "Coarse Track" due to the aero-optical distortion present. This result is consistent with the visual observations made in Figure 11.

We extend the analysis to computing the *Aero MTF* for these image sequences as follows,

$$Aero\ MTF = \frac{Fine\ Track\ MTF}{No\ Flow\ MTF} = \frac{Coarse\ Track\ MTF}{NoFlow\ MTF}. \tag{6}$$

The results are shown on a logarithmic x-axis plot in Figure 12(b). As expected, the blue line of "No Flow'' is consistent at MTF of 100%. The red stars represent the "Fine Track" and the orange stars present the "Coarse Track". We expect to see the "Fine Track" points resulting in slightly higher MTF contrast than the "Coarse Track" points, however, the plot is sparse and clear trend is difficult to discern. Based on the challenges encountered in

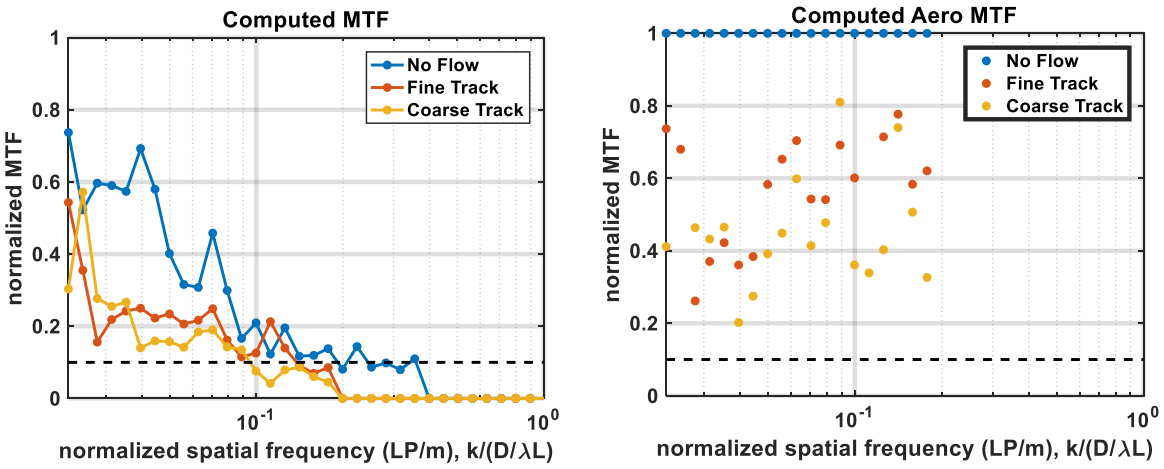

(a) (b)

Figure 12. (a) MTF computed from flight images (b) *Aero MTF* computed from the MTF curves. The results are shown on a logarithmic x-axis because the ROI is within the largest spatial frequencies.

this flight experiment, we recommend the following enhancements to minimize uncertainity in the *Aero MTF* calculations. First, the captured image should avoid having resolution elements impacted by vignetting. Image processing can correct for some of these optical distortions, but also introduces other manipulation errors. Second, three line resolution elements are rotation dependent. Rotating an image introduces interpolation artifacts that slightly blur the image. Since we are measuring a subtle effect any artificial blurring due to processing should be avoided. A rotation invariant pattern would eliminate this issue. Third, blurring due to jitter is magnified with increasing range. Jitter effects that are insignificant at $L = 50m$ become prominent when the aircraft separation is tripled to $L = 150m$. Lastly, the spatial frequencies of the aircraft target board are heavily dependent on a precise range of $L = 150m$. Even a change of a few meters in separation results in significant shifts in the normalized spatial frequency MTF plots. Measuring the separation via GPS would allow for precisely adjusting the range in the MTF calculations for each image capture. The following experiment builds on these lessons and enhances the aero imaging flight data.

4.3 Experiment 3: Flight Campaign with Spoke Pattern and GPS

The experiment was performed on the AAOL-T consisting of two aircraft flying in close formation with a nominal 50m separation. The separation range was modified from 150m to 50m to improve the imaging capabilities. To perform in-flight measurements of image degradation due to aero-optical effects, a target board, shown in Figure 13, top right, was placed on the side window of the laser aircraft, around the outgoing laser beam. A rectangular

horizontal cut in the middle of the target board allowed the laser beam to be transmitted to the laboratory aircraft over a range of viewing angles. The new target board consisted of a collection of patterns of three parallel bars with various lengths, widths and orientations, similar to the ones in the USAF 1951 target board, so that image blurring could be measured to directly obtain the MTF. In addition, two spoke patterns were present on the target board, providing a continuous and redundant rotation-independent means of extracting MTF.[7]

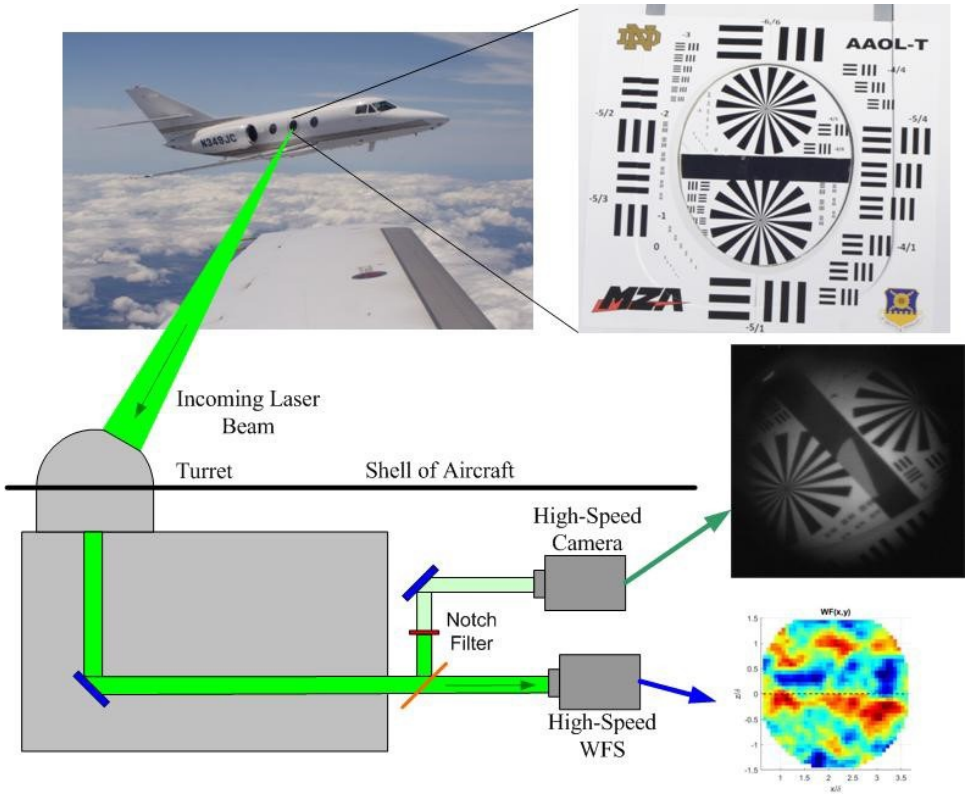

Figure 13. The schematic of the simultaneous wavefront-imaging flight experiment.

Both the incoming laser beam, aberrated by the aero-optical distortions over the turret, and the reflected light from the target board were transmitted through the turret optical system. The received light was split between the two high-speed sensors. To collect time-resolved wavefronts, a Shack-Hartmann sensor was used. The Shack-Hartmann wavefront sensor consists of the lenslet array mounted on a high-speed Phantom v711 camera. The wavefronts were acquired at 20 kHz with the exposure time of 0.4 μsec for 16,000 frames with a spatial resolution of 36x36 subapertures.

The time-resolved imaging of the scoring board, illuminated by the ambient light from the Sun, was collected using a Phantom v1611 camera. To prevent the incoming laser beam from damaging the camera, a dichroic notch filter was used. The lens for the imaging camera had an adjustable focal length from 150-500 mm with a minimum f-stop of 8. The 2x teleconverter (doubler) was attached to the lens to double the effective focal length. For the actual images, the lens was set to a focal length of 300 mm, giving an effective focal length of 600 mm, and the f-stop was set to the minimum value of 8 to maximize the incoming light. The images of the scoring board were taken at 1 kHz with the exposure time of 1 msec for 5,000 frames. As the beam jitter due to mechanical motion of the turret was found to be present mostly over low frequencies below 400 Hz,[4] images were collected at the higher sampling speed of 1 kHz to attempt to minimize the image blurring due to beam jitter but still giving an exposure time that was large enough to collect relatively bright images.

Both cameras were triggered simultaneously to ensure their synchronization. The sampling allowed both instantaneous wavefronts and blurred images to be collected simultaneously. The Phanton v1611 camera was

manually focused before each data point acquisition. The flights were performed over Mach numbers between 0.5 and 0.8 and different altitudes and turret viewing angles between 80 and 150 degrees. The distance between the aircraft was measured using a differential GPS-system, capable to measuring the distance to better than 1 cm, and the distance was maintained at to be close to a nominal distance of $L = 50m$. The flight parameters such as local flow angle of attack and static and total pressure were also acquired simultaneously with the wavefronts and imaging data, using angle-of-attack probe, installed on the laboratory aircraft.

In general, it is expected that larger aero-optical distortions will result in blurrier images. Simultaneous wavefronts and images were collected in flight, Figure 14 shows imagery captured at forward-looking LOSangle 100° and backward-looking LOSangle 140°. We observe that the vignetting is remains an issue, and neither spoke pattern is full captured within the image. When processing the MTF of the spoke pattern, we select the pattern more prominently visible for processing. This is usually the spoke pattern located below the laser slot. The automated processing uses the center of the spoke pattern as reference and compute modulations along circles of various radius lengths. Each radius represent a different spatial frequency. Thus, since at $L = 50m$ the full radius of the spoke pattern is 200 pixels, we obtain 200 MTF points on the normalized spatial frequency axis. This a notable increase from the 33 points measured in Experiment 2. For each circle, we locate the maximum intensity and look for the local minimum within two modulations of the maximum intensity. This allows us to avoid the dark vignetted regions of the image. All the MTF scores are computed from the brightest center region of the image. Once a max and min has been determined for a defined spatial frequency circle, we use Equation 2 to compute the contrast score.

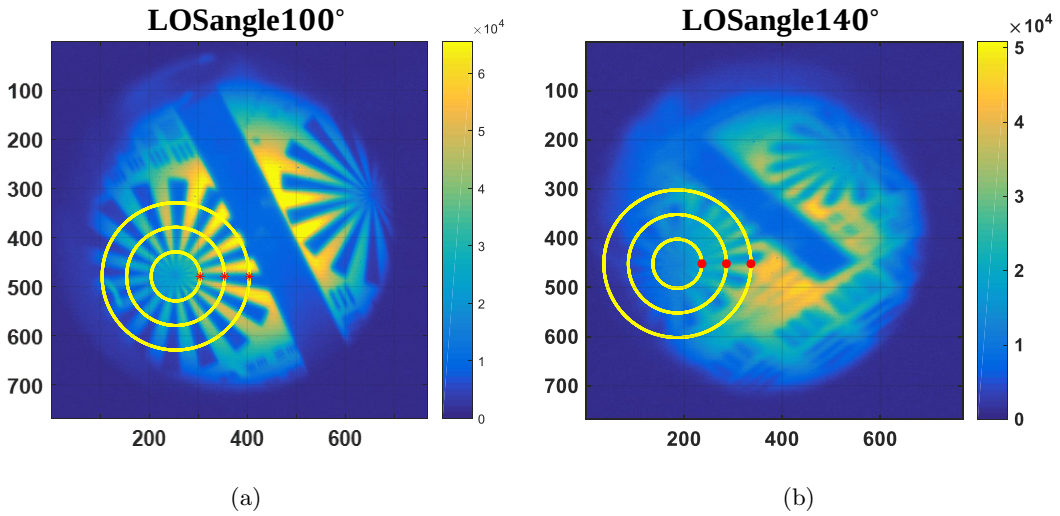

(a) (b)

Figure 14. (a) LOSangle 100° contains minor aero-optical distortions. (b) LOSangle 140° contains significant blur due to aero-optical image degradation.

The images capture in this experiment allow us to more accurately compute the MTF of an image sequence. In Figure 14(a), we visually observe high contrast between the white spokes and dark spokes. The yellow rings represent radius values of $R = 50$, 100, and 150. Since LOSangle 100° is close to ideal orthogonality (90°), each circle correctly represents a single spatial frequency. LOSangle 100° is forward-looking and contains low aero-optical distortions. In Figure 14(b), the image blur is more prominent. There are several distortion effecting the image. First, the aero-optic effect is more significant at LOSangle 140° and causes blurriness. Second, the capture target board is no longer orthogonal to the camera, therefore we observe distortions from the elongated nature of the spoke pattern.

During the collection the aircraft positions with respect to one another drifts, and therefore the image coordinates of spoke pattern change from frame to frame. The MTF processing script involves registering all the subsequent frames to the position of the first frame. In this way, we can obtain an initial spoke pattern

position using the first frame and all other frames will use the same spoke pattern coordinates. For each frame of a captured sequence, we can can compute a MTF curve. Since all our collections captured 5,000 frames, we compute 5,000 MTF curves per sequence. The average MTF of the LOSangle 100° (red) and LOSangle 140° (blue) are shown in Figure 15. The plot is focused on the largest spatial frequencies from 0.0 to 0.1 of (λ/D_{ap}). The quantifiable aero-optic imaging effects are seen been the red and the blue curve. For all spatial frequencies the LOSangle 100° show higher contrast score than the distorted LOSangle 140° case. We note that there is a dip in the MTF curve for low spatial frequencies of the LOSangle 140° case. This occurs due to the misalignment of the MTF processing circles with the spoke pattern. At low spatial frequencies, the large circles fall outside the spoke pattern, and therefore register lower contrast modulation. To quantify the imaging performance, we sum all the MTF points to measure the area under the curve. Larger areas are associated with better image quality. Additional analysis of aero-optical effects around the turret in-flight and the discussion of the relation between statistical properties of these effects and the resulted image blurring is provided in the companion paper.[7]

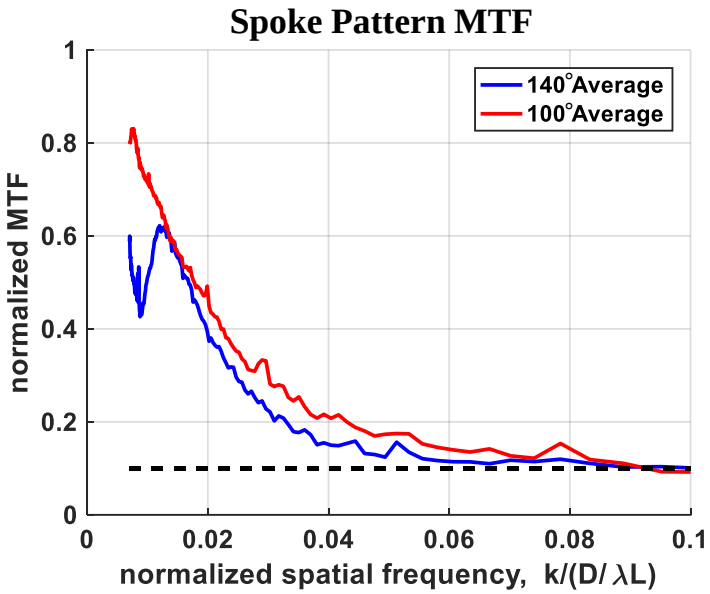

Figure 15. Quantifying the aero-optical effects. Average computed MTFs for image sequences captured at LOSangle 100° with minor aero optic effects and LOSangle 140° greater aero-optical effects.

4.4 Lessons for Future Aero-Optic Imaging Flights

Having completed two aero-optic imaging flight campaigns we have compiled a list of important lessons and notes for future aero-optic imaging experiments. We recommend the following for future aero-optic imaging tests:

1. **Optimize the Turret Optics.** We learned that the MTF of the aero-optical effects is subtle and requires precise imaging capabilities to accurately measure the aero impact. The quality of the optics and imaging system provided a baseline starting point from which we measure the aero-optical degradation. Imaging artifacts, as vignetting and dimming, can have a severe effect on the appearance of the resolution target. Image processing can correct for some of these optical distortions, but also introduces other manipulation errors in the process.

2. **Utilize Continuous Rotation Invariant Resolution Target Boards.** The MTF calculations are susceptible to rounding and pixelization errors, therefore we recommend maximizing the quantity of spatial frequencies measured. Unlike the 33 MTF points available from the three-line-element target board in Section 4.2, the spoke pattern provided us with 200 points of varying spatial frequency. Also, since we are measuring a subtle effect any artificial blurring due to processing should be avoided. Our spoke pattern target board is a rotation invariant pattern that eliminate this rotation dependency issue.

3. **Minimize Jitter.** We have taken several steps to minimize residual jitter artifacts. Residual jitter causes image blurring that can be mistaken for aero-optical distortions. We found that when the high frequency feedback control loop of the "Fine Tracking" turret operation mode is engaged the residual jitter is significantly reduced compared to the "Coarse Tracking" mode. As a result, less blurring due to jitter is accumulated in the collect images. Secondly, we must balance the camera parameters between higher sample rates and exposure times. Images should be collected at the higher sampling speed (1 to 4 kHz) to attempt to minimize the image blurring due to beam jitter (mechanical motion is 400Hz) but still allow for an exposure time that collects sufficiently bright images. Thirdly, blurring due to jitter is magnified with increasing range. Jitter effects that are insignificant at $L = 50m$ become prominent when the aircraft separation is tripled to $L = 150m$. We plan to continue to fly at $L = 50m$ aircraft separation.

4. **Use a Differential GPS for Separation Measurements.** The spatial frequencies of the aircraft target board are heavily dependent on a precise range. Even a change of a few meters in separation results in significant shifts in the normalized spatial frequency MTF plots. Measuring the separation via GPS is critical for precisely adjusting the range in the MTF calculations for each image capture.

5. **Time Syncing All System Components.** Each data points is collected for approximately 1 second in duration. It is important for the analysis that all collect data is representing the same aero disturbances. Both cameras were triggered simultaneously to ensure their synchronization. We recommend time sync the system clocks with the wavefront sensor, camera, and differential GPS measurements.

6. **Collect Various Ground Data for a "No Aero" Baseline.** As shown in Section 4.1, determining the *Aero MTF* is measured by dividing the in-flight distorted image MTF by the ground "No Aero" MTF. In order to have consistency in the computed MTFs, we suggest placing a strong emphasis on the baseline ground data. Ideally, the ground data should contain numerous LOSangles which would be have the same non-orthogonal image skewing as the in-flight data for those LOSangles. Our image processing scripts can simulate the image skewing but also simultaneously introduces minor interpolation artifacts.

7. **Autofocus the Turret using GPS Data.** An important caveat in the presented experiments is that the Phanton v1611 camera was manually focused before each data point acquisition. Even with ideal focus at the begin of a data point collection, the focus of the imaging system is sensitive to the aircraft separation range. Although the aircrafts maintain a nominal $L = 50m$ separation there is continuous back and forth drift in the range which can quickly defocus the collection. Automating this focusing process to be a function of the measured differential GPS distance would eliminate any potential operator error and add consistency to the collected imagery.

8. **Quantify the Impact of Aero Mitigation Techniques on Imaging Performance.** Measuring and quantifying the aero-optical image degradation is the first step to determining the optimal aero-mitigation needed for imaging through a turret. Our future experiments will focus on evaluating the mitigation configurations and evaluate imaging performance for various LOSangles.

Many of these recommendations (marked 1 to 4) have already been incorporated into the AAOL-T system configuration. Our future work is focused on implementing the remaining recommendations to obtain more accuracy and precision in our aero-optic imaging sensors and processing algorithms.

5 CONCLUSIONS

We presented modeling and simulation techniques for computing the blurring effects on images due to aero-optical distortions around hemispherical turrets. The technique for computing the modulation transfer function from images was validated against wavefront point spread functions and optical transfer function calculations. The MTF is used to quantify the imaging performance. Three experiments in which we evaluated the imaging performance of the AAOL-T turret were presented. The first experiment evaluated the USAF-1951 target board indoors to quantify the imaging performance with out aero-optical distortions. The second experiment consisted of imaging a large three-line-element resolution target board in-flight. Two turret operation modes, "Fine Tracking" and "Coarse Tracking", were evaluated. The third experiment was a second flight campaign using the AAOL-T

program aircrafts for simultaneously imaging a spoke pattern resolution target and collecting the instantaneous aberrating wavefronts due to the turbulent flow around the turret. Using time-resolved wavefronts, point spread functions and modulation transfer functions were calculated for different turret viewing angles.

Our results show that aero-optical image distortion can be quantified using our MTF technique. Future work will include refinement of the processing algorithm and further automation of the collection process. As noted in the analysis, the aero-optical degradation is subtle and sensitive, therefore precision in the optics, acquisition, and processing is required.

ACKNOWLEDGMENTS

This work is supported by the Joint Technology Office, Grant number FA9550-13-1-0001. The U.S. Government is authorized to reproduce and distribute reprints for governmental purposes notwithstanding any copyright notation thereon.

REFERENCES

[1] Goorskey, D. J., Schmidt, J., and Whiteley, M. R., "Efficacy of predictive wavefront control for compensating aero-optical aberrations," Optical Engineering **52**(7), 071418–071418 (2013).

[2] Sutton, G. W., "Optical imaging through aircraft turbulent boundary layers," Aero-Optical Phenomena **80**, 15–39 (1982).

[3] Jumper, E. J. and Fitzgerald, E. J., "Recent advances in aero-optics," Progress in Aerospace Sciences **37**(3), 299–339 (2001).

[4] Jumper, E. J., Gordeyev, S., Cavalieri, D., Rollins, P., Whiteley, M., and Krizo, M., "Airborne aero-optics laboratory-transonic (aaol-t)," AIAA Paper **675**, 2015 (2015).

[5] Gordeyev, S., Burns, R., Jumper, E., Gogineni, S., Paul, M., and Wittich, D., "Aero-optical mitigation of shocks around turrets at transonic speeds using passive flow control," in [51st AIAA Aerospace Sciences Meeting], 2013–0717 (2013).

[6] Whiteley, M. R. and Goorskey, D. J., "Imaging performance with turret aero-optical wavefront disturbances," Optical Engineering **52**(7), 071410–071410 (2013).

[7] Gordeyev, S., DeLucca, N., Diskin, Y., Jumper, E., and Whiteley, M., "Image blurring due to turbulent wakes for airborne systems: Flight tests," SPIE Optical Engineering Applications, San Diego, CA (Aug. 6-10, 2017) .

[8] Jumper, E. J., Zenk, M. A., Gordeyev, S., Cavalieri, D., and Whiteley, M. R., "Airborne aero-optics laboratory," Optical Engineering **52**(7), 071408–071408 (2013).

[9] Goorskey, D. J., Drye, R., and Whiteley, M. R., "Dynamic modal analysis of transonic airborne aero-optics laboratory conformal window flight-test aero-optics," Optical Engineering **52**(7), 071414–071414 (2013).

[10] Whiteley, M. R., Goorskey, D. J., and Drye, R., "Aero-optical jitter estimation using higher-order wavefronts," Optical Engineering **52**(7), 071411–071411 (2013).

[11] Whiteley, M. R. and Gordeyev, S., "Conformal phased array aero-optical modeling and compensation," Optical Engineering **52**(7), 071409–071409 (2013).

[12] Goodman, J. W., [Introduction to Fourier optics], Roberts and Company Publishers (2005).

[13] Morrida, J., Gordeyev, S., and Jumper, E., "Transonic flow dynamics over a hemisphere in flight," AIAA Paper **1349**, 2016 (2016).

[14] Born, M. and Wolf, E., "Principles of optics (pergamon press, oxford)," Pergamon Press **6**, 188–189 (1980).

[15] Holst, G. C., [Electro-optical imaging system performance], JCD Pub. (1995).

[16] Standard, M., "Photographic lenses," Washington, DC: Armed Forces Supply Support Center (1959).

[17] Krizo, M. J., Cusumano, S. J., Fiorino, S. T., Heap, R., Velten, V., Brown, J., and Bartell, R. J., "Design, development, and in-flight testing of a pointer/tracker for in-flight experiments to measure aero-optical effects over a scaled turret," Optical Engineering **52**(7), 071415–071415 (2013).